Chapter 11

Statistical Image Texture Analysis

ROBERT M. HARALICK
Machine Vision International
Ann Arbor, Michigan

INTRODUCTION I

The advent of automatic image analysis resulted in two fundamentally different approaches to texture analysis: the statistical approach and the structural approach. The statistical approach generates parameters to characterize the stochastic properties of the spatial distribution of gray levels in an image. The structural approach analyzes visual scenes in terms of the organization and relationships among its substructures. In this chapter we present a survey of the representative literature regarding statistical texture analysis. However, we do include references to structural techniques for completeness. Thorough reviews of texture models and approaches have been presented by Haralick [1] and Ahuja and Rosenfeld [2].

HANDBOOK OF PATTERN RECOGNITION
AND IMAGE PROCESSING

Ehrich and Foith [3] summarize the main issues in texture analysis. These issues are listed in the general historical order that researchers have been concerned with them.

(1) Given a textured region, determine to which of a finite number of classes does the region belong.
(2) Given a textured region, determine a description or model for it.
(3) Given an image having many textured areas, determine the boundaries between the differently textured regions.

Issue (1) has to do with the pattern recognition task of texture feature extraction. Issue (2) has to do with generative models of texture. Issue (3) has to do with using what we know about issues (1) and (2) in order to perform a texture segmentation of an image. In the remainder of this section we provide a brief historical elaboration of issues (1) and (2).

Early work in image texture analysis sought to discover useful features that had some relationship to the fineness and coarseness, contrast, directionality, roughness, and regularity of image texture. Tamuro, Mori, and Yamawaki [4] discuss the relationship of such descriptive measures to human visual perception. Typically, an image known to be texturally homogeneous was analyzed, and the problem was to measure textural features by which the image could be classified. For example, using microscopic imagery, discrimination between eosinophils and large lymphocytes was accomplished by using a texture feature for cytoplasm and a shape feature of the cell nucleus [5]. By using aerial imagery, discrimination of areas having natural vegetation and trees from areas having man-made objects, buildings, and roads [6] was accomplished using textural features. These statistical textural feature approaches included use of the autocorrelation function, the spectral power density function, edgeness per unit area, spatial gray-tone co-occurrence probabilities, gray-tone run-length distributions, relative extrema spatial distributions, and mathematical morphology.

Later approaches to image texture analysis sought a deeper understanding of what image texture is by the use of a generative image model. Given a generative model and the values of its parameters, it is possible to synthesize homogeneous image texture examples associated with the model and the given value of its parameters. This association provides a theoretical and visual means of understanding the texture. Image texture analysis then amounts to verification and estimation. First, it must be verified that a given image texture sample is consistent with or fits the model. Then the values of the model parameters must be estimated on the basis of the observed sample. Autoregressive moving-average time-series models (extended to two dimensions), Markov random fields, and mosaic models are examples of some of the model-based techniques.

In Section II we give a brief illustration of texture examples. Section III is the body of the paper and reviews and classifies the published literature on statistical texture analysis.

TEXTURE EXAMPLES II

To motivate our discussion of image texture, we illustrate how texture manifests itself on aerial imagery. We will see from these examples that spatial environments can be understood as being spatial distributions of various area-extensive objects having characteristic size and reflectance or emissive qualities and that the spatial organization and relationships of the area-extensive objects appear as gray-tone spatial distributions on imagery taken of the environment.

Figure 2, taken from Lewis [9], illustrates how texture relates to geomorphology. Here, we examine some plains, low hills, high hills, and mountains in the Panama and Columbia area as seen on some Westinghouse AN/APQ97 *K*-band radar imagery.

The plains have apparent relief of 0–50 m, the hills have apparent relief of 50–350 m, and the mountains have apparent relief of more than 350 m. The low hills have little dissection and are generally smooth, convex surfaces, whereas the high hills are highly dissected and have prominent ridge crests.

The mountain texture is distinguishable from the hill texture on the basis of the extent of radar shadowing (black tonal areas). The mountains have shadowing over more than half the area and the hills have shadowing over less than half the area. The hills can be subdivided from low to high on the basis of the abruptness of tonal change from terrain front slope to terrain back slope.

Figure 2, taken from McDonald [7], illustrates how texture relates to geology. Here, we examine some igneous and sedimentary rocks in Panama as seen on some Westinghouse AN/APQ97 *K*-band radar imagery. Figures 2i,k,l show a fine-textured drainage pattern, which is indicative of nonresistant, fine-grained sedimentary rocks. The coarser texture of Figure 2h, left and diagonal, is indicative of coarse-grained sediments. A massive texture with rugged and peaked divides (Figs. 2a,b,c,d,e) is indicative of igneous rocks. When erosion has nearly base leveled an area, the texture takes on the hummocky appearance of Fig. 2c.

Figure 3, taken from Haralick and Anderson [8], illustrates how texture relates to land use categories. Here, we examine five land use categories as they appear on panchromatic aerial photography. Notice how the texture of the wooded area is coarser and more definite than the scrub area. The swamps and marsh generate finer textures than those generated from wood

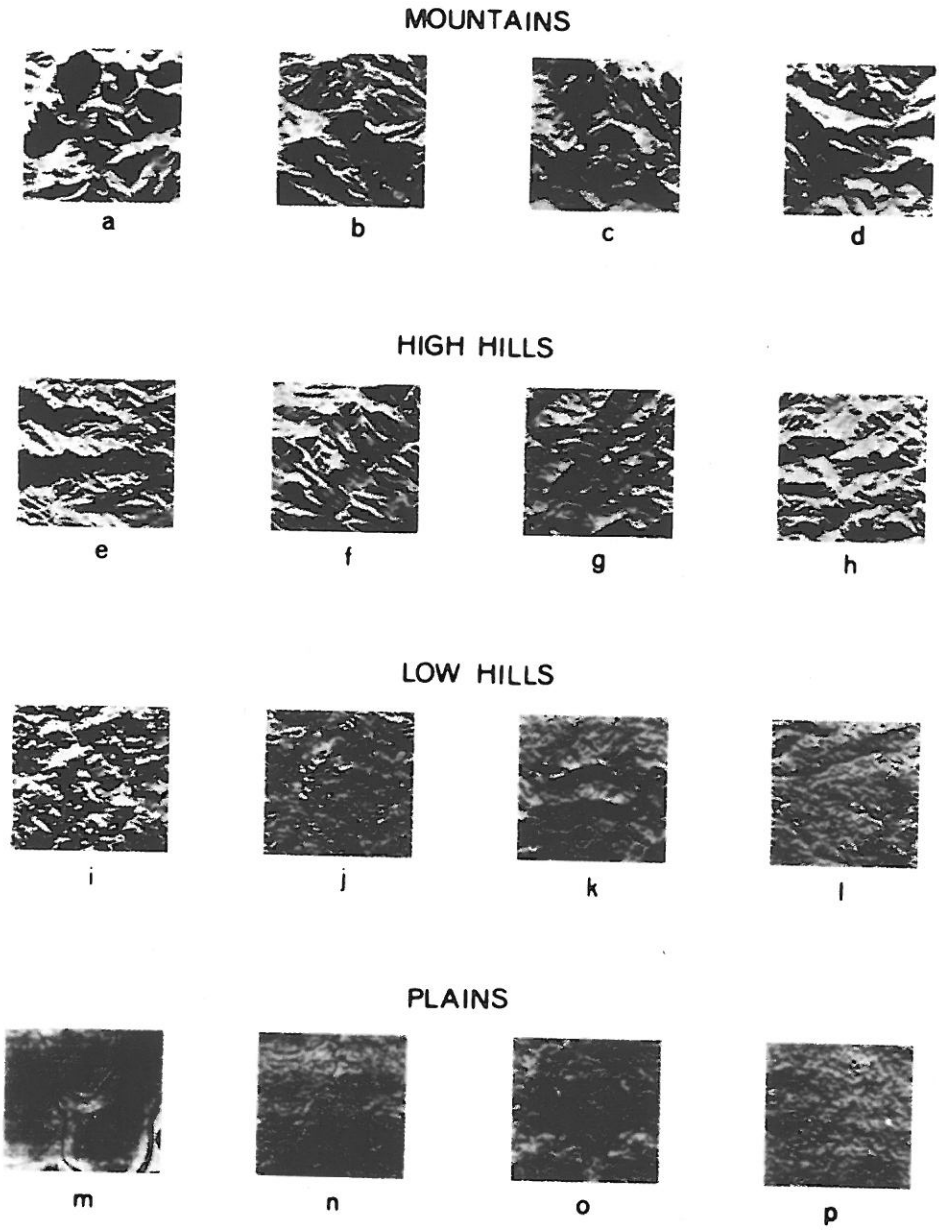

Fig. 1. *K*-band radar imaging illustrating how texture relates to geomorphology. (From Lewis [9].)

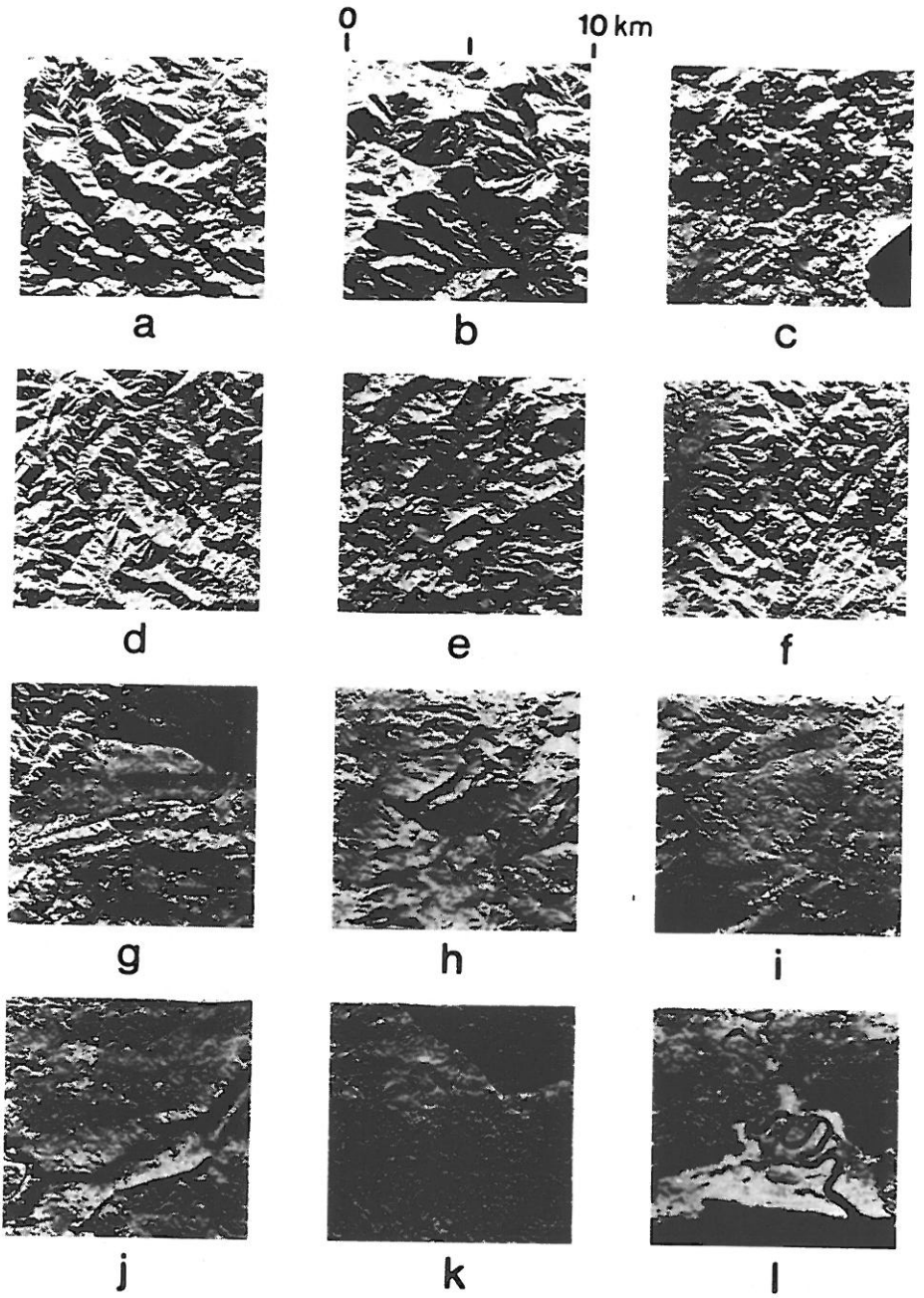

Fig. 2. Textures generated by igneous and sedimentary rocks on *K*-band radar imagery. (From McDonald [7].)

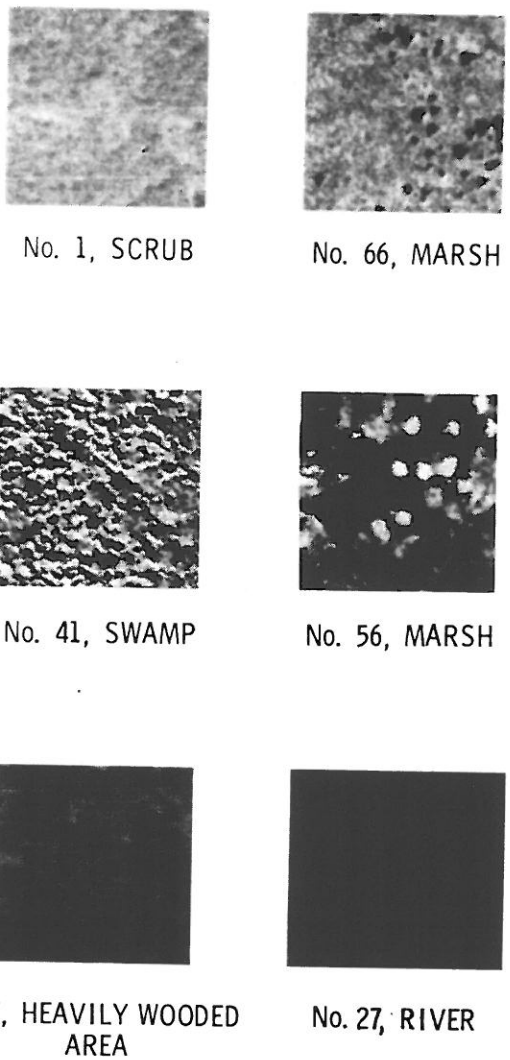

Fig. 3. Natural-environmental scenes illustrating how texture relates to land use categories in panchromatic aerial photography. No. 1, ETL No. 815-N2; No. 66, ETL No. 43-T3B; No. 41, ETL No. 43-TB; No. 56, ETl No. 53-T3A; No. 7, ETL No. 697-N1A; No. 27, ETL No. 88-R. (From Haralick and Anderson [8].)

or scrub areas. The swamp texture is finer and shows more gradual gray-tone change than the marsh-generated textures.

Figures 4–6 illustrate how the same environment can generate a variety of textures within the same texture type. Figure 4 shows five environments where the vegetation both increases in size and disperses. Figure 5, taken in the Pisgah Crater area, shows five environments where the vegetation

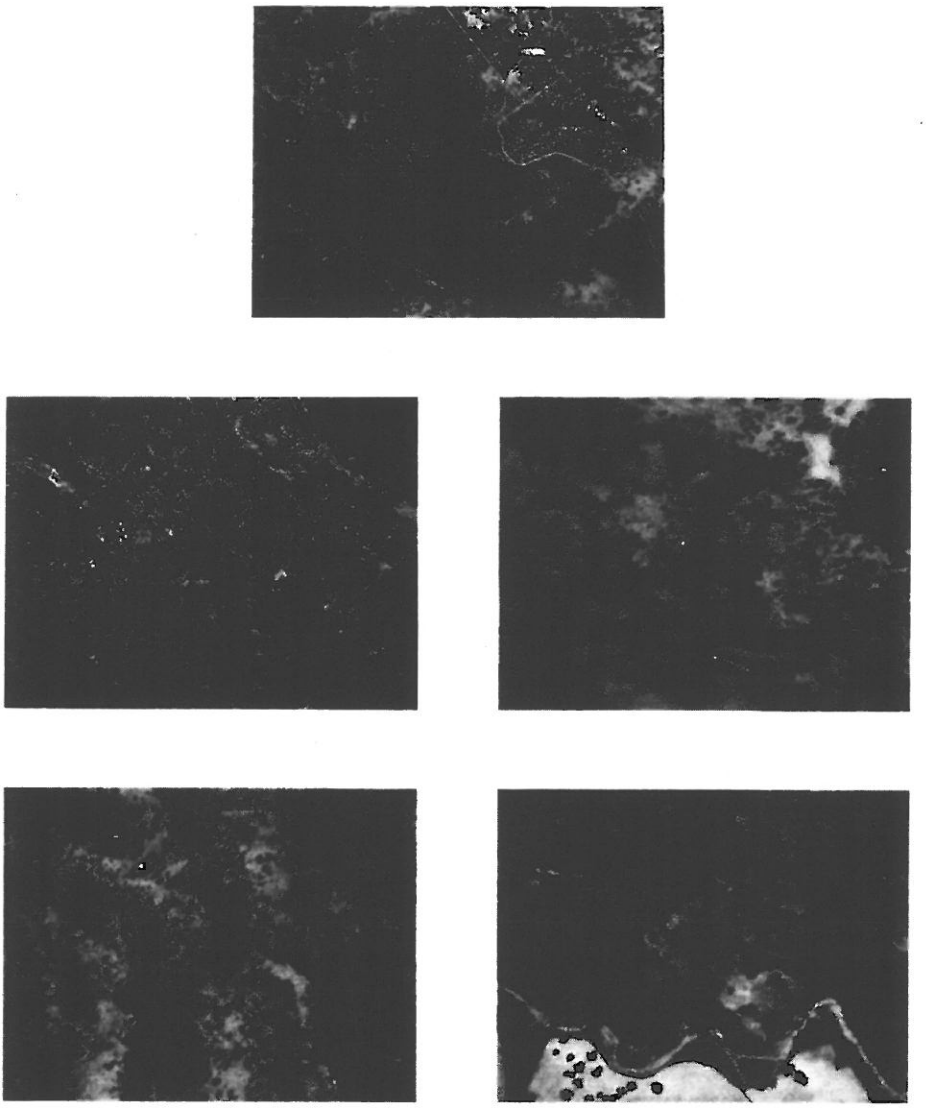

Fig. 4. Illustration of how the size and spacing of vegetation can cause texture to change from fine to coarse.

increases in size, probably due to greater available soil moisture. Figure 6, taken in the Pisgah Crater area, shows five environments of lava beds having increasingly distinct contrast.

In these examples it is clear that texture relates to land types and classification. Furthermore, any one land use type may generate a range of textures in the same texture grade on a scale of strong to weak, fine to coarse, etc.

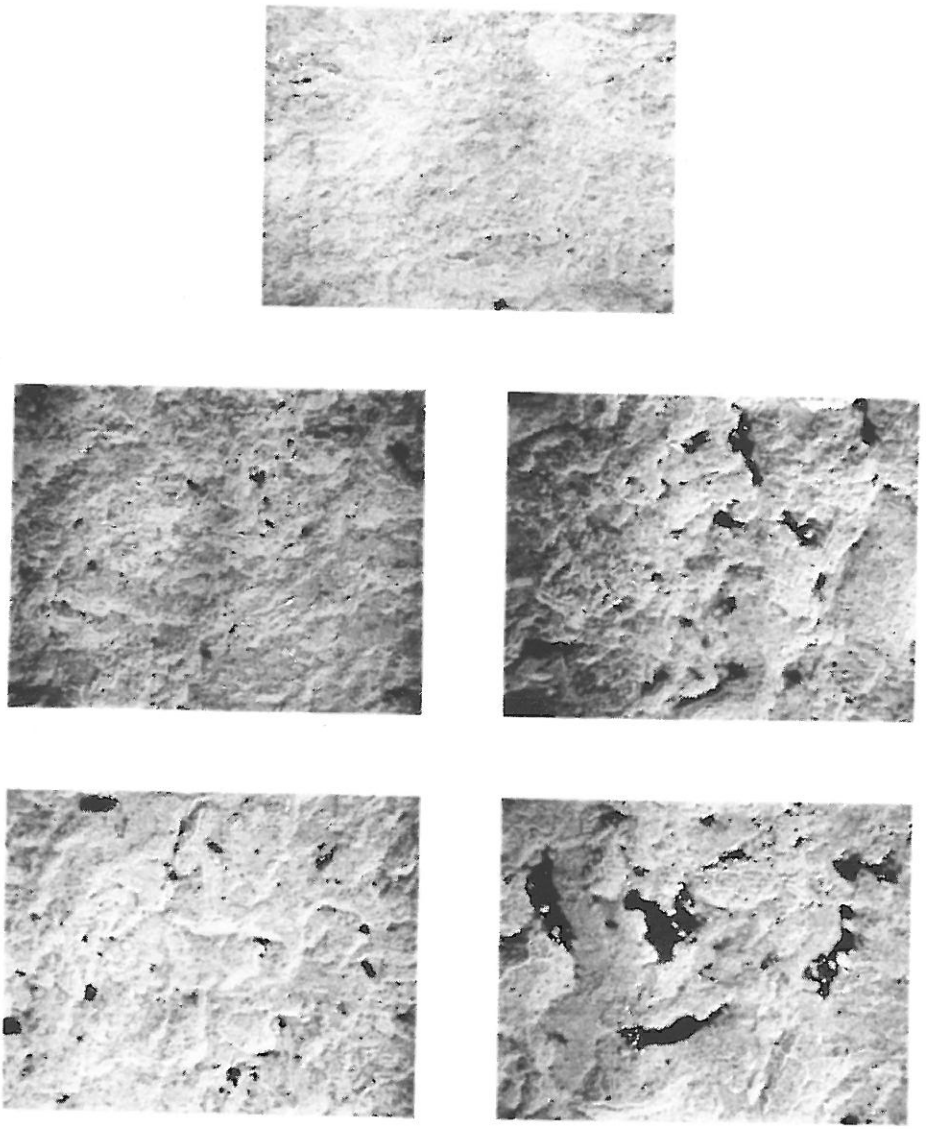

Fig. 5. Negative images illustrating how the same kind of lava can have a different texture.

III STATISTICAL TEXTURE FEATURES

In this section we survey the following techniques of statistical textural measures: autocorrelation, orthogonal transforms, gray-tone co-occurrence, mathematical morphology, gradient analysis, relative extrema density, three-dimensional shape from texture, discrete Markov random fields, random mosaic models, and texture segmentation. In addition, we give a brief discussion of synthetic-texture image generation.

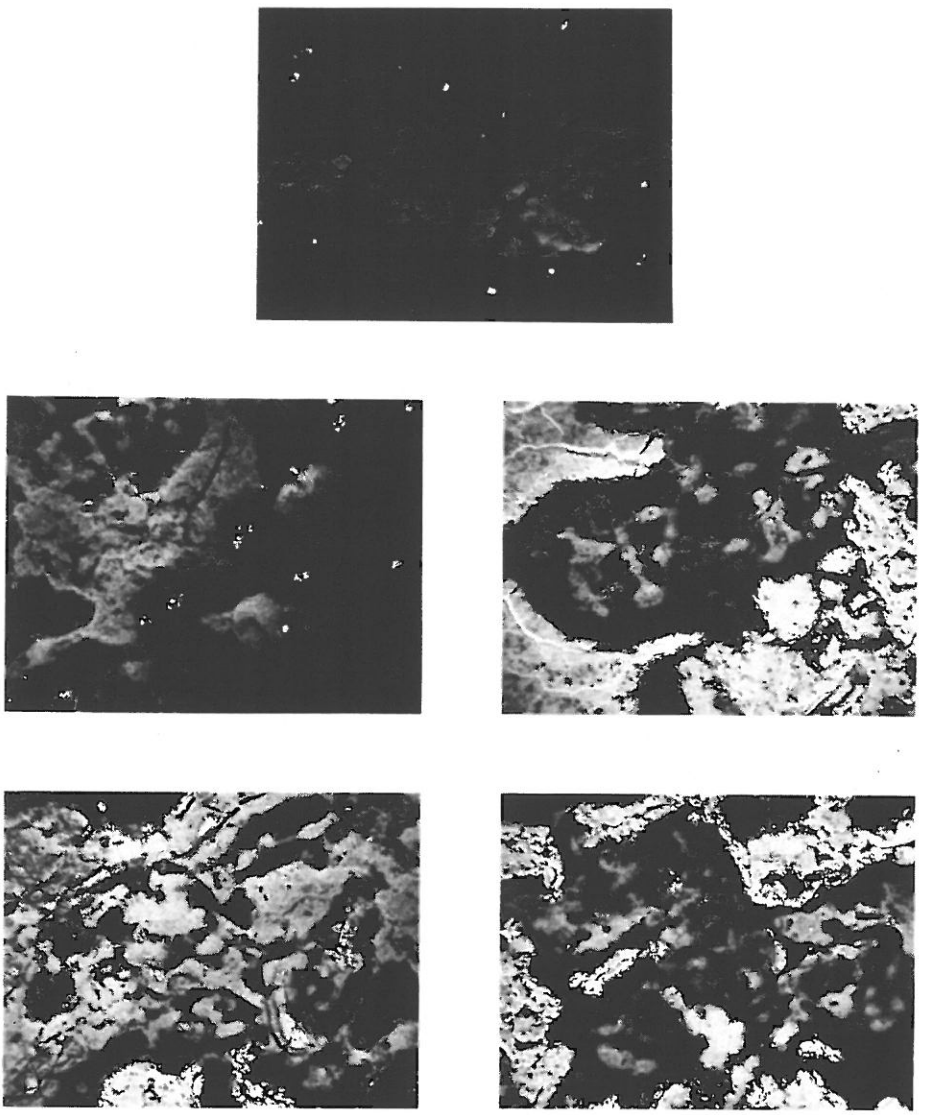

Fig. 6. Negative images illustrating how lava can have different textures.

The Autocorrelation Function and Texture A

From one point of view, texture relates to the spatial size of the tonal primitives on an image. Tonal primitives of larger size are indicative of coarser textures; tonal primitives of smaller size are indicative of finer textures. The autocorrelation function is a feature which tells about the size of the tonal primitives.

We describe the autocorrelation function with the help of a thought

experiment. Consider two image transparencies which are exact copies of one another. Overlay one transparency on top of the other, and with a uniform source of light, measure the average light transmitted through the double transparency. Now translate one transparency relative to the other and measure only the average light transmitted through the portion of the image where one transparency overlaps the other. A graph of these measurements as a function of the (x, y) translated positions and normalized with respect to the $(0, 0)$ translation depicts the two-dimensional autocorrelation function of the image transparency.

Let $I(u, v)$ denote the transmission of an image transparency at position (u, v). We assume that outside some bounded rectangular region $0 \leq u \leq L_x$ and $0 \leq v \leq L_y$ the image transmission is zero. Let (x, y) denote the 0 translation. The autocorrelation function ρ for the image transparency I is formally defined by

$$\rho(x, y) = \frac{\dfrac{1}{(L_x - |x|)(L_y - |y|)} \displaystyle\int_{-\infty}^{\infty}\int I(u, v)I(u + x, v + y)\, du\, dv}{\dfrac{1}{L_x L_y} \displaystyle\int_{-\infty}^{\infty}\int I^2(u, v)\, du\, dv}$$

where $|x| < L_x$ and $|y| < L_y$. Here we are assuming the image has mean 0.

If the tonal primitives on the image are relatively large, then the autocorrelation will drop off slowly with distance. If the tonal primitives are small, then the autocorrelation will drop off quickly with distance. To the extent that the tonal primitives are spatially periodic, the autocorrelation function will drop off and rise again in a periodic manner. The relationship between the autocorrelation function and the power spectral density function is well known: they are Fourier transforms of one another [10].

The tonal primitive in the autocorrelation model is the gray tone. The spatial organization is characterized by the correlation coefficient, which is a measure of the linear dependence one pixel has on another pixel displaced from it by the vector (x, y).

An experiment was carried out by Kaizer [11] to see if the autocorrelation function had any relationship to the texture that photointerpreters see in images. He used a series of seven aerial photographs of an Arctic region and determined the autocorrelation function of the images with a spatial correlator that worked in a manner similar to the one envisioned in our thought experiment. Kaizer assumed the autocorrelation function was circularly symmetric and computed it only as a function of radial distance. Then, for each image, he found the distance d such that the autocorrelation function ρ at d took the value $1/e$ (i.e., $\rho(d) = 1/e$).

Kaizer then asked 20 subjects to rank the 7 images on a scale from fine detail to coarse detail. He correlated the rankings with the distances

corresponding to the $(1/e)$th value of the autocorrelation function. He found a correlation coefficient of 0.99. This established that, at least for his data set, the autocorrelation function and the subjects were measuring the same kind of textural features.

Kaizer noticed, however, that even though there was a high degree of correlation between $\rho^{-1}(1/e)$ and subject rankings, some subjects put first what $\rho^{-1}(1/e)$ put fifth. Upon further investigation, he discovered that a relatively flat background (indicative of high frequency or fine texture) can be interpreted as a fine-textured or coarse-textured area. This phenomena is not unusual and actually points out a fundamental characteristic of texture: it cannot be analyzed without a reference frame of tonal primitive being stated or implied. For any smooth gray-tone surface, there exists a scale such that when the surface is examined, it has no texture. Then, as resolution increases, it takes on a fine texture and then a coarse texture. In Kaizer's situation, the resolution of his spatial correlator was not good enough to pick up the fine texture which some of his subjects did in an area that had a weak but fine texture.

Orthogonal Transformations B

Spatial frequency characteristics of two-dimensional images can be expressed by the autocorrelation function or by the power spectra of those images. Both may be calculated digitally and/or implemented in a real-time optical system.

Lendaris and Stanley [12, 13] used optical techniques to perform texture analysis on a database of low-altitude photographs. They illuminated small circular sections of those images and used the Fraunhoffer diffraction pattern to generate features for identifying photographic regions. The major discriminations of concern to these investigators were those of man-made roads, intersections of roads, buildings, and orchards.

Feature vectors extracted from these diffraction patterns consisted of 40 components. Twenty of the components were mean energy levels in concentric annular rings of the diffraction pattern, and the other 20 components were mean energy levels in 9° wedges of the diffraction pattern. Greater than 90% classification accuracy was reported using this technique.

Cutrona, Leith, Palermo, and Porcello [14] present a review of optical processing methods for computing the Fourier transform. Goodman [15], Preston [16], and Shulman [17] also present comprehensive reviews of Fourier optics in their books. Swanlund [18] discusses the hardware specifications for a system using optical techniques to perform texture analysis.

Gramenopoulos [19] used a digital Fourier transform technique to analyze aerial images. He examined subimages of 32×32 pixels and determined that for a LANDSAT image over Phoenix, spatial frequencies between 3.5 and 5.9 cycles/km contained most of the information required to

discriminate among terrain types. An overall classification accuracy of 87% was achieved using image categories of clouds, water, desert, farms, mountain, urban, river bed, and cloud shadows. Horning and Smith [20] used a similar approach to interpret aerial multispectral scanner imagery.

Bajscy [21] and Bajscy and Lieberman [22, 23] computed the two-dimensional power spectra of a matrix of square image windows. They expressed the power spectrum in a polar coordinate system of radius versus angle. They determined that directional textures tend to have peaks in the power spectrum along a line orthogonal to the direction of the texture. Bloblike textures tend to have peaks in the power spectrum at radii associated with the sizes of the blobs. This work also shows that texture gradients can be measured by determining the trends of relative maxima of radii and angles as a function of the position of the image window whose power spectrum is being analyzed. For example, as the power peaks along the radial direction tend to shift toward larger values, the image surface becomes more finely textured.

In general, features based on Fourier power spectra have been shown to perform more poorly than features based on second-order gray-level co-occurrence statistics [24] or those based on first-order statistics of spatial gray-level differences [25, 26]. The presence of aperture effects has been hypothesized to account for part of the unfavorable performance by Fourier features compared to space-domain gray-level statistics [27], although experimental results indicate that this effect, if present, is minimal. However, D'Astous and Jernigan [28] argue that the reason for the poorer performance is that earlier studies using the Fourier transform features used summed spectral energies within band- or wedge-shaped regions in the power spectrum. They argue that additional discriminating information can be obtained from the power spectrum in terms of characteristics such as regularity, directionality, linearity, and coarseness. The degree of regularity can be measured by the relative strength of the highest non-dc peak in the power spectrum. Other peak features include the Laplacian at the peak, the number of adjacent neighbors of the peak containing at least 50% of the energy in the peak, the distance of the peak from the origin, and the polar angle of the peak. In the comparative experiment reported by D'Astous and Jernigan, the peak features yielded uniformly greater interclass difference than the co-occurrence features, and the co-occurrence features yielded uniformly greater interclass distances than the summed Fourier energy features.

Pentland [29] computed the discrete Fourier transform for each block of 8×8 pixels of an image and determined the power spectrum. He then used a linear regression technique on the log of the power spectrum as a function of frequency to estimate the fractal dimension D. For gray-tone intensity surfaces of textured scenes which satisfy the fractal model [30], the power spectrum satisfies

$$P(f) = Cf^{-1(2D+1)}$$

Pentland reported a classification accuracy of 84.4% on a texture mosaic using fractal dimensions computed in two orthogonal directions.

Transforms other than the Fourier transform can be used for texture analysis. Kirvida [31] compared the fast Fourier, Hadamard, and Slant transforms for textural features on aerial images of Minnesota. Five classes (hardwood trees, conifers, open space, city, and water) were studied using 8×8 subimages. A 74% correct classification rate was obtained using only spectral information. This rate increased to 98.5% when textural information was also included in the analysis. These researchers reported no significant difference in the classification accuracy as a function of which transform was employed.

The simplest orthogonal transform that can be locally applied is the identity transformation. Lowitz [32, 33] and Carlotto [34] suggest using the local histogram for textural feature extraction. Lowitz uses window sizes as large as 16×16. Corlotto uses window sizes as large as 33×33.

Gray-Tone Co-Occurrence C

Textural features can also be calculated from a gray-level spatial co-occurrence matrix. The co-occurrence (Pi, j) of gray tones i and j for an image I is defined as the number of pairs of resolution cells (pixels) having gray levels i and j, respectively, and which are in a fixed spatial relationship, such as a fixed distance apart or a fixed distance and a fixed angle. The co-occurrence matrix can be normalized by dividing each entry by the sum of all of the entries in the matrix. Conditional probability matrices can also be used for textural feature extraction, with the advantage that these matrices are not affected by changes in the gray-level histogram of an image, only by changes in the topological relationships of gray levels within the image.

Formally, let S be the set of all pairs of pixels in the given spatial relation. Then

$$P(m, n) = |\{((i, j), (k, l)) \in S | I(i, j) = m \text{ and } I(k, l) = n\}|$$

Zucker [35] suggested using a distance d for the spatial relationship which maximizes a chi-square statistic of P. Julesz [36] was the first to use co-occurrence statistics in visual human texture discrimination experiments. Zobrist and Thompson [37] used co-occurrence statistics in a Gestalt grouping experiment. Darling and Joseph [38] used statistics obtained from nearest-neighbor gray-level transition probability matrices to measure textures using spatial intensity dependence in satellite images taken of clouds. Deutsch and Belknap [39] used a variant of co-occurrence matrices to describe image texture. Bartels and Wied [40], Bartels *et al.* [41], and Wied *et al.* [42] used one-dimensional co-occurrence statistics for the analysis of

cervical cells. Rosenfeld and Troy [43], Haralick [44], and Haralick *et al.* [24] suggested the use of spatial co-occurrence for arbitrary distances and directions. Galloway [45] used gray-level run-length statistics to measure texture. These statistics are computable from co-occurrence assuming that the image is generated by a Markov process. Chen and Pavlidis [46] used the co-occurrence matrix in conjunction with a split-and-merge algorithm to segment an image at textural boundaries. Tou and Chang [47] used statistics from the co-occurrence matrix, followed by a principal components eigenvector dimensionality reduction scheme, to reduce the dimensionality of the classification problem.

Statistics that Haralick *et al.* [24] compute from such co-occurrence matrices of equal-probability quantized images (see also Conners and Harlow [48]) have been used to analyze textures in satellite images [49]. An 89% classification accuracy was obtained. Additional applications of this technique include the analysis of microscopic images [6], pulmonary radiographs [50], and cervical cell, leukocyte, and lymph node tissue section images [51, 52].

Commonly used statistics of the co-occurrence probabilities include energy, entropy, contrast, correlation, and homogeneity. They are defined as

$$\text{Energy} \qquad \sum_i \sum_j P(i,j)^2$$

$$\text{Entropy} \qquad \sum_i \sum_j P(i,j) \log P(i,j)$$

$$\text{Contrast} \qquad \sum_i \sum_j (i-j)^2 P(i,j)$$

$$\text{Correlation} \qquad \sum_i \sum_j (i-u_x)(j-u_y)P(i,j) \Big/ \sigma_x \sigma_y$$

$$\text{Homogeneity} \qquad \sum_i \sum_j \frac{P(i,j)}{1+|i-j|}$$

Vickers and Modestino [53] argue that using features of the co-occurrence matrix in a classification situation is surely suboptimal and that better results would be obtained by using the co-occurrence matrix directly in a maximum-likelihood classifier. They report better than 95% correct identification accuracy in distinguishing between tree bark, calf leather, wool, beach sand, pigskin, plastic bubbles, herringbone weave, raffia, and wood grain textures.

Bacus and Gose [5] used a gray-tone difference variant of the co-occurrence matrix to help distinguish between eosimophils and lymphocytes. They used the probability of a given contrast occurring in a given spatial relationship as a textural feature. This gray-tone difference probability can be defined in terms of the co-occurrence probabilities by

$$P(d) = \sum_i \sum_j P(i,j), \qquad |i-j| = d$$

For a coarse texture, the probability of a small contrast d will be much higher than the probability of a small contrast for a fine texture. Bacus and Gose used statistics of the differences between a pixel on a red image and a displaced pixel on a blue image. Rosenfeld *et al.* [54] also suggest using multispectral difference probabilities. Haralick and Shanmugam [24] used multispectral co-occurrence probabilities.

Weszka *et al.* [25] used the contrast, energy, entropy, and mean of $P(d)$ as texture measures and report that they do about as well as the co-occurrence probabilities. Sun and Wee [55] suggested a variant of the gray-level difference distribution. They fix a distance d and a contrast c and determine the number of pixels each having gray tone g and each having n neighbors that are within distance d and within contrast c. That is,

$$P(g, n) = \#\{(i, j) | I(i, j) = g \text{ and } \#\{(k, l) | \rho((i, j), (k, l)) \leq d \text{ and } |I(i, j) - I(k, l)| \leq c\} = n\}$$

From $P(g, n)$ they compute a variety of features, such as entropy and energy. They report an 85% classification accuracy on distinguishing between textures of three different geological terrain types on Landsat imagery. Wechsler and Kidode [56] and Wechsler and Citron [57] used the gray-tone difference probabilities to define a random-walk model for texture. See DeSouza [58] and Percus [59] for some comments about the random-walk model.

Haralick [60] illustrated a way to use co-occurrence matrices to generate an image in which the value at each resolution cell is a measure of the texture in the resolution cell's neighborhood. All of these studies produced reasonable results on different textures. Conners and Harlow [61, 26] concluded that this spatial gray-level dependence technique is more powerful than spatial frequency (power spectra), gray-level difference (gradient), and gray-level run-length methods [45] of texture quantitation.

Dyer *et al.* [62] and Davis *et al.* [63] computed co-occurrence features for local properties such as edge strength maxima and edge direction relationships. They suggested computing gray-tone co-occurrence only involving those pixels near edges. Zucker and Kant [64] also suggested using generalized co-occurrence statistics. Terzopoulos and Zucker [65] reported a 13% increase in accuracy when combining gray-tone co-occurrence features with edge co-occurrence features in the diagnosis of osteogenesis imperfecta from images of fibroblast cultures.

Davis [66] computed co-occurrence probabilities for spatial relationships parameterized by angular orientation. He defined the polarogram to be a statistic of these co-occurrence probabilities as a function of the angular orientation. See also Chetverikov [67]. Chetverikov [68] used co-occurrence statistics as a function of displacement to determine texture regularity.

D Mathematical Morphology

Mathematical morphology is the study of shape. For texture analysis, the shapes analyzed are the shapes of the tonal primitives. The morphological approach to the texture analysis of binary images was proposed by Matheron [69] and Serra and Verchery [70]. This approach requires the definition of a structuring element (i.e., a set of pixels constituting a specific shape, such as a line, a disk, or a square) and the generation of binary images, which result from the translation of the structuring element through the image and the erosion of the image by the structuring element. The textural features can be obtained from the new binary images by counting the number of pixels having the value 1. This mathematical morphology approach of Serra and Matheron is the basis of the Leitz Texture Analyser (TAS) [71–73] and the Cyto Computer [74]. A broad spectrum of applications has been found for this quantitative analysis of microstructures method in materials science and biology.

Watson [75] summarizes this approach to texture analysis. Let H, a subset of resolution cells, be the structuring element. We define the translate of H by row–column coordinates (r, c) as $H(r, c)$, where

$$H(r, c) = \{(i, j) | \text{ for some } (r', c') \in H, i = r + r', j = c + c'\}$$

Then the erosion of F by the structuring element H, written $F \ominus H$, is defined as

$$F \ominus H = \{(m, n) | H(m, n) \subseteq F\}$$

The eroded image J obtained by eroding F with structuring element H is a binary image where pixels take the value 1 for all resolutions cells in $F \ominus H$. Textural properties can be obtained from the erosion process by appropriately parameterizing the structuring element (H) and determining the number of elements of the erosion as a function of the parameter's value.

For example, a two-pixel structuring element can be parameterized by fixing a row distance and column distance between two pixels. The normalized area of the erosion as a function of row and column distance is the autocorrelation function of the binary image. Another one-parameter structuring element is a disk. Another is a one-pixel width annulus. The parameter in both cases is the radius. The area of the eroded image as a function of the parameter provides a statistical description of the shape distribution of the image.

The dual operation to erosion is dilation. The dilation of F by structuring element H, written $F \oplus H$, is defined by

$$F \oplus H = \{(m, n) | \text{for some } (i, j) \in F \text{ and } (r, s) \in H, \quad m = i + r \text{ and } n = j + s\}$$

Compositions of erosions and dilations determine two other important morphological operations which are idempotent and are duals of one

another: openings and closings. The opening of F by H is defined by $(F \ominus H) \oplus H$. The closing of F by H is defined by $(F \oplus H) \ominus H$.

The number of binary 1 pixels of the opening as a function of the size parameter of the structuring element can determine the size distribution of the grains in an image. We just take H_d to be a line-structuring element of length d or a disk-structuring element of diameter d. We can then define the granularity of the image F by

$$G(d) = 1 - \frac{|(F \ominus H_d) \oplus H_d|}{|F|}$$

where $|F|$ means the number of elements in F. $G(d)$ measures the properties of grain pixels which cannot be contained in some translated structuring element of size d which is entirely contained in the grain and which contains the given pixel. Thus, it measures the proportion of pixels participating in grains having a size smaller than d.

Sternberg [76] has extended the morphological definition of erosion to gray-tone images. The erosion of gray-tone image I by gray-tone structuring element H produces a gray-tone image J which is defined by

$$J(r, c) = \min_{(i,j)}\{I(r + i, c + j) - H(i, j)\} = (I \ominus H)(r, c)$$

The dilation of gray-tone image I by gray-tone structuring element H produces a gray-tone image J which is defined by

$$J(r, c) = \max_{(i,j)}\{I(r - i, c - j) + H(i, j)\} = (I \oplus H)(r, c)$$

The gray-tone opening is defined as a gray-tone erosion followed by a gray-tone dilation. The gray-tone closing is defined as a gray-tone dilation followed by a gray-tone erosion. Commonly used gray-tone structuring elements include rods, disks, cones, paraboloids, and hemispheres.

Peleg *et al.* [77] use gray-tone erosion and dilation to determine the fractal surface of the gray-tone intensity surface of a textural scene. They define the scale k volume of the blanket around a gray-tone intensity surface I to be

$$V(k) = \sum_{(r,c)} (I \oplus H^k)(r, c) - (I \ominus H^k)(r, c)$$

where H^k is the dilation of H with itself k times and H is defined over the five-pixel cross neighborhood, taking the value of 1 for the center pixel and 0 elsewhere. The fractal surface area A at scale k is then defined by

$$A(k) = [V(k) - V(k - 1)]/2$$

The fractal signature S at scale k is then defined by

$$S(k) = \frac{d}{d \log k} \log A(k) = \frac{kA'(k)}{A(k)}$$

They compare the similarity between textures by the weighted distance D between their fractal signatures:

$$D = \sum_k (S_1(k) - S_2(k))^2 \log\left[\frac{k + (1/2)}{k - (1/2)}\right]$$

Werman and Peleg [78] give a fuzzy set generalization to the morphological operators. Meyer [79] and Lipkin and Lipkin [80] have demonstrated the capability of morphological textural parameters in biomedical image analysis. Theoretical properties of the erosion operator as well as other operators are presented by Matheron [81], Serra [82, 83], and Lantuejoul [84]. The importance of this approach to texture analysis is that properties obtained by the application of operators in mathematical morphology can be related to physical three-dimensional shape properties of the materials imaged.

E Gradient Analysis

Rosenfeld and Troy [43] and Rosenfeld and Thurston [85] regard texture in terms of the amount of "edge" per unit image area. An edge can be detected by a variety of local mathematical operators which essentially measure some property related to the gradient of the image intensity function. Rosenfeld and Thurston use the Roberts gradient and then compute, as a measure of texture for any image window, the average value of the Roberts gradient taken over all of the pixels in the window. Sutton and Hall [86] extend this concept by measuring the gradient as a function of the distance between pixels. An 80% classification accuracy was achieved by applying this textural measure in a pulmonary disease identification experiment.

Related approaches include Triendl [87], who smoothed the image using 3×3 neighborhood, then applied a 3×3 digital Laplacian operator, and finally smoothed the image with an 11×11 window. The resulting texture parameters obtained from the frequency-filtered image can be used as a discriminatory textural feature. Hsu [88] determines edgeness by computing variance-like measures for the intensities in a neighborhood of pixels. He suggested as a textural feature the deviation of the intensities in a pixel's neighborhood from both the intensity of the central pixel and from the average intensity of the neighborhood. The histogram of a gradient image was used to generate texture properties of the nuclei of leukocytes by Landeweerd and Gelsema [89]. Rosenfeld [90] generated an image whose intensity is proportional to the edge per unit area of the original image. This transformed image is then further processed by gradient transformations prior to textural feature extraction. Harris and Barrett [91] used vector

dispersion as a feature to identify cloud types. They reported a 72% identification accuracy. Lu *et al* [92] used a 2 × 2 operator which estimates the second mixed partial derivative to make the resulting image be stationary, and they then used a first-order autoregressive moving-average model to describe the texture of the filtered image. Carlotto [34] computed the gradient and gradient angle at each pixel and used the histograms of these for textural features. Shen and Wong [93] similarly used the local gradient and gradient angle histogram for a variety of window sizes.

Relative Extrema Density F

Rosenfeld and Troy [43] suggested the number of extrema per unit area for a texture measure. They defined extrema in a purely local manner, allowing plateaus to be considered as extrema. Ledley [94] and Rotolo [95] also suggested computing the number of extrema per unit area as a texture measure. They, as well as Mitchell *et al.* [96], suggested operating on a smoothed image to eliminate extrema due to noise. (See also Carlton and Mitchell [97] and Ehrich and Foith [3, 98].

One problem with simply counting all extrema in the same extrema plateau as extrema is that extrema per unit area is not sensitive to the difference between a region having a few large plateaus of extrema and many single-pixel extrema. The solution to this problem is to only count an extrema plateau once. This can be achieved by locating some central pixel in the extrema plateau and marking it as the extrema associated with the plateau. Another way of achieving this is to associate a value $1/N$ for every extrema in an N-pixel extrema plateau.

In the one-dimensional case, there are two properties that can be associated with every extrema: its height and its width. The height of a maximum can be defined as the difference between the value of the maxima and the highest adjacent minimum. The height (depth) of a minimum can be defined as the difference between the value of the minimum and the lowest adjacent maximum. The width of a maximum is the distance between its two adjacent minima. The width of a minimum is the distance between its two adjacent maxima. Osmon and Saukar [99] use the mean and standard deviation of the spacing between relative extrema to characterize the surface texture of materials.

Two-dimensional extrema are more complicated than one-dimensional extrema. One way of finding extrema in the full two-dimensional sense is by the iterated use of some recursive neighborhood operators propagating extrema values in an appropriate way. Maximally connected areas of relative extrema may be areas of single pixels or may be plateaus of many pixels. We can mark each pixel in a relative extrema region of size N with the value h,

indicating that it is part of a relative extrema having height h, or mark it with the value h/N, indicating its contribution to the relative extrema area. Alternatively, we can mark the most centrally located pixel in the relative extrema region with the value h. Pixels not marked can be given the value 0. Then for any specified window centered on a given pixel, we can add up the values of all pixels in the window. This sum divided by the window size is the average height of extrema in the area. Alternatively, we could set h to 1 and the sum would be the number of relative extrema per unit area to be associated with the given pixel.

Going beyond the simple counting of relative extrema, we can associate properties to each relative extremum. For example, given a relative maximum, we can determine the set of all pixels reachable only by the given relative maximum and not by any other relative maxima by monotonically decreasing paths. This set of reachable pixels is a connected region and forms a mountain. Its border pixels may be relative minima or saddle pixels.

The relative height of the mountain is the difference between its relative maximum and the highest of its extractor border pixels. its size is the number of pixels which constitute it. Its shape can be characterized by features such as elongation, circularity, and symmetric axis. Elongation can be defined as the ratio of the larger to smaller eigenvalue of the 2×2 second-moment matrix obtained from the coordinates of the border pixels [100, 101]. Circularity can be defined as the ratio of the standard deviation to the mean of the radii from the center of the region to its border [60]. The symmetric axis feature can be determined by thinning the region down to its skeleton and counting the number of pixels in the skeleton. For regions that are elongated, it may be important to measure the direction of the elongation or the direction of the symmetric axis.

G Shape from Texture

Image texture gradients on oblique photography can be used to estimate the surface orientation of the observed three-dimensional object. The first work of this kind was done by Carel *et al.* [102] and Charton and Ferris [103]. They did a conceptual design of a system called VISILOG, which could direct a freely moving vehicle through an undetermined environment. One important kind of guidance information needed by such a vehicle is the surface orientation of the surface over which the vehicle is moving. The basis of the design was an analysis that related surface slant to the texture gradient in the perspective projection image. Assumptions were that a stochastically regular surface is observed through a perspective projection and the number of texture elements could be measured along two parallel line segments perpendicular to the view direction and two parallel line segments parallel to

the view direction. They measured the number of texture elements in a line by measuring the number of changes in brightness along the line. The number of changes in brightness is the number of relative extrema.

Witkin [104], apparently unaware of the earlier work, derived equations for the slant and tilt angle of a planar surface under orthographic projection by measuring the distribution of tangent direction of zero-crossing contours. Witkin divided the tangent angle interval $[0, \pi]$ into n equal intervals, the ith interval being $[(i-1)\pi/n, i\pi/n]$ $(i = 1, \ldots, n)$, and measured the number $k(i)$ of tangent directions that fall in the ith interval. The slant angle s and the tilt angle t of the observed surface is estimated to be that pair of values maximizing the a posteriori probability of (s, t) given the observed $k(i)$, $i = 1, \ldots, n$. Davis *et al.* [105] indicated some mistakes in the Witkin paper and give the joint a posteriori probability of (s, t) as proportional to

$$P(s, t/k(i), \ldots, k(n)) = \alpha \sin s \cos^n s / \prod_{i=1}^{n} \left\{ 1 - \sin^2 s \sin^2 \left[\frac{(2i-1)\pi}{2n} - t \right] \right\}$$

They also gave a modified version of the two-dimensional Newton method for determining the (s, t) achieving the maximization.

Other work that relates to surface orientation recovery from texture includes that of Kender [106], who described an aggregation Hough-related transform that groups together edge directions associated with the same vanishing point. An edge direction $E = (E_x, E_y)$ at position $P = (P_x, P_y)$ has coordinates $T = (T_x, T_y)$ in the transformed space where

$$T = \frac{\mathbf{E} \cdot \mathbf{P}}{\mathbf{E} \cdot \mathbf{E}} E$$

Discrete Markov Random Fields H

The Markov random-field model for texture assumes that the texture field is stochastic, stationary, and satisfies a conditional independence assumption. Let $\mathbf{R} \times \mathbf{C}$ be the spatial domain of an image, and for any $(r, c) \in \mathbf{R} \times \mathbf{C}$ let $N(r, c)$ denote the neighbors of (r, c). Because the field is stationary, $(a, b) \in N(r, c)$ if and only if $(a + i, c + j) \in N(r + i, c + j)$. This means that the spatial neighborhood configuration is the same all over the image. There is an obvious difficulty with this condition holding at pixels near the image boundary. The usual way of handling the problem theoretically is to assume the image is wrapped around a torus. In this case, the canonical spatial neighborhood can be given as $N(0, 0)$.

The conditional independence assumption is that the conditional probability of the pixel given all the remaining pixels in the image is equal to the

conditional probability of the pixel given just the pixels in its neighborhood. That is,

$$P(I(r, c)|I(i, j): (i, j) \in \mathbf{R} \times \mathbf{C}, (i, j) \neq (r, c)) = P(I(r, c)|I(i, j): (i, j) \in N(r, c))$$

Markov mesh models were first introduced into the pattern recognition community by Chow [107] and then Abend, *et al.* [108]. One important issue is how to compute the joint probability function $P(I(r, c): (r, c) \in \mathbf{R} \times \mathbf{C})$. Hassner and Sklansky [109] note that this can be done by identifying the conditional probability assumption with Gibbs ensembles, which are studied in statistical mechanics. Woods [110] showed that when the distributions are Gaussian, the discrete Gauss-Markov field can be written as an equation in which each pixel's value is a linear combination of the values in its neighborhood plus a correlated noise term. That is,

$$I(r, c) = \sum_{(i, j) \in N(0, 0)} I(r - i, c - j)h(i, j) + u(r, c)$$

where the coefficients of the linear combination are given by the function h and $\{u(r, c)|(r, c) \in \mathbf{R} \times \mathbf{C}\}$ represent a joint set of possible correlated Gaussian random variables. This equation has a lot of similarity to the autoregressive moving-average time-series models of Box and Jenkins [111]. Here the relationship would be expressed by

$$I(r, c) = \sum_{(i, j) \in N(0, 0)} I(r - i, c - j)h(i, j) + \sum_{(i, j) \in N(0, 0)} u(r - i, c - j)k(i, j)$$

where $N(0, 0)$ represents a domain which contains only pixels occurring after $(0, 0)$ in the usual top-down raster scan order of an image. Hence, each term in the summation $I(r - i, c - j)$ contains only pixels occurring before pixel (i, j) in the raster scan order. The first summation is called the autoregressive term and the second term is called the moving-average term. When $N(0, 0)$ contains pixels occurring before and after $(0, 0)$ in the raster scan order, the model is called a simultaneous autoregressive model.

It is apparent that the discrete Markov random-field model is a generalization of time-series autoregressive moving-average models, which were initially explored for image texture analysis by McCormick and Jayaramamurthy [112], Tou and Chang [113], Tou *et al.* [114], and Deguchi and Morishita [115]. Related papers include Delp *et al.* [116], Tou [117], Chen [118], Faugeras [119], Therrien [120], and Jau *et al.* [121]. Issues concerning the estimation of h from texture samples can be found in Kashyap and Challappa [122]. DeSouza [123] develops a chi-square test to discriminate microtextures described by autoregressive models.

Pratt [124], Pratt *et al.* [125], and Faugeras and Pratt [126] consider only

the autoregressive term with independent noise and rewrite the autoregressive equation as

$$I(r, c) - \sum_{(i,j)\in N(0,0)} I(r-i, c-j)h(i, j) = u(r, c)$$

Here, $\{u(r, c) | (r, c) \in \mathbf{R} \times \mathbf{C}\}$ represents independent random variables, not necessarily Gaussian. The left-hand side represents a convolution which decorrelates the image. Faugeras and Pratt characterize the texture by the mean, variance, skewness, and kurtosis of the decorrelated image, which is obtained either by estimating h or by using a given gradient- or Laplacian-like operator to perform the decorrelation.

Another related approach is the texture energy transform approach described by Laws [127]. Laws applied a variety of linear operators on an image. Each operator had a small neighborhood for its domain. The squared operator outputs were then averaged with an equally weighted running-average window having a larger spatial domain than the original operators. The resulting values constituted the textural feature vector at each pixel. In the comparative experiment Laws performed, the co-occurrence features yielded an identification accuracy of 72%. The texture energy transform approach yielded an identification accuracy of 87%. Unser [128] noted that one could use a discrete orthogonal transform such as the discrete sine or discrete cosine transforms applied locally to each pixel's neighborhood instead of using the ad hoc linear operators of Laws. He indicated a classification accuracy above 96% with the discrete sine transform in distinguishing between textures of paper, grass, sand, and raffia. Ikonomopoulos and Unser [129] suggested local directional filters. Jernigan and D'Astous [130] computed a fast Fourier transform on windows and then used the entropy in different-sized regions for the normalized power spectrum for textural features.

Random Mosaic Models

The random mosaic models are constructed in two steps. The first step provides a means of tessellating a plane into cells, and the second step assigns a property value to each cell. In the Poisson line model [131], the plane is tessellated by a random set of lines. Each cell is then a connected region whose boundary consists of line segments from the lines in the random set. In the occupancy model [132], a tesselation is produced by a random process which plants points in the plane. Each point determines a cell which consists of all points in the plane closest to the given planted point. In the Delauney model, a line segment is drawn between each pair of planted points whose corresponding cells in the occupancy model share a common border segment.

Schachter *et al.* [133] and Schachter and Ahuja [134] derived the statistical properties for these random mosaic models. Ahuja, *et al.* [135] compared properties of synthetically generated textures with their theoretical values. Schachter [136] summarized how texture characteristics are related to the texture's variogram and correlation function. Modestino *et al.* [137, 138] computed the power spectral density function for a plane tesselated by a random line process and in which the gray levels of one cell have a Markov dependence on the gray levels of the cells around them. They gave a maximum-likelihood texture discriminant for this mosaic model and illustrated its use on some sample images. Therrien [139] used an autoregressive model for each cell and, like Modestino *et al.* [137, 138], superimposed a Markov random field to describe transitions between cells. Other models include the Johnson–Mehl model [140] and the bombing model [141].

J Texture Segmentation

Most work in image texture analysis has been devoted to texture feature analysis of an entire image. However, it is apparent that an image is not necessarily homogeneously textured. An important image processing operation, therefore, is the segmentation of an image into regions, each of which are homogeneously textured. The constraint is that each pair of adjacent regions is differently textured. Bajcsy [142] was one of the first researchers to do texture segmentations for outdoor scenes. Her algorithm merged together small, nearly connected regions having similar local texture or color descriptors. For texture descriptors she used Fourier transform features. The descriptors for each region included an indication of whether the texture is isotropic or directional, the size of the texture element, and the separation between texture elements. If the texture was considered directional, then the description included the orientation.

Chen and Pavlidis [46] used the split-and-merge algorithm on the co-occurrence matrix of regions as the basis for merging. Let the four $2^{N-1} \times 2^{N-1}$ windows in a $2^N \times 2^N$ window have C^{NE}, C^{NW}, C^{SE}, and C^{SW} for their respective co-occurrence matrices. Then, with only little error, the co-occurrence matrix C of the $2^N \times 2^N$ window can be computed by

$$C(i,j) = \tfrac{1}{4}[C^{NE}(i,j) + C^{NW}(i,j) + C^{SE}(i,j), C^{SW}(i,j)]$$

Experiments done by Hong *et al.* [143] indicate that the error of this computation is minimal. The $2^N \times 2^N$ window is declared to be uniformly textured if, for the user specified threshold T,

$$\sum_{(i,j)} \max\{C^{NE}(i,j), C^{NW}(i,j), C^{SE}(i,j), C^{SW}(i,j)\}$$

$$-\min\{C^{NE}(i,j), C^{NW}(i,j), C^{SE}(i,j), C^{SW}(i,j)\} < T$$

Using this criteria Chen and Pavlidis begin the merging process using 16 × 16 windows. Any 16 × 16 window not merged is split into four 8 × 8 windows. The splitting continues until the window size is 4 × 4. The gray tones of the images were quantized to eight levels. Chen and Pavlidis [144] used a similar split-and-merge algorithm, with the correlation coefficients between vertically adjacent and horizontally adjacent pixels as the feature vectors. Modestino *et al.* [138] used a Poisson line process to partition the plane and assign gray levels to each region by a Gauss–Markov model using adjacent regions. They developed a maximum-likelihood estimator for the parameters of the process and show segmentation results on artificially generated images having three different texture types.

Connors, *et al.* [145] use six features from the co-occurrence matrix to segment an aerial urban scene into nine classes: residential, commercial/industrial, mobile home, water, dry land, runway/taxiway, aircraft parking, multilane highway, and vehicle parking. Their work is important because it combined the splitting idea of Chen and Pavlidis into a classification setting. Any window whose likelihood ratio for its highest likelihood class against any other class is too low is considered a boundary region and split. Any window whose likelihood ratio for its highest likelihood class against each other class is high enough is considered to be uniformly textured and assigned to the highest likelihood class.

Kashyap and Khotanzad [146] used a simultaneous autoregressive and circular autoregressive model for each 3 × 3 neighborhood of an image. Here each neighborhood produced a feature vector associated with the model. The set of feature vectors generated from the image was clustered and each pixel was labeled with the cluster label of the feature vector associated with its 3 × 3 neighborhood. Pixels associated with outlier feature vectors are given the cluster label of the majority of its labeled neighbors. Therrien [139] used an autoregressive model for each textured region and superimposed a Markov random field to describe the transitions of one region to another. He used maximum likelihood and maximum a posteriori estimation techniques to achieve a high-quality segmentation of aerial imagery.

K Synthetic-Texture Image Generation

There have been a variety of approaches to the generation of synthetic-texture images. Rather than giving a detailed description of each, we just provide a brief guide to some of the representative papers in the literature. McCormick and Jayaramamurthy [112] used a time-series model for texture synthesis, as do Tou *et al.* [114]. Yokoyama and Haralick [147] used a structured growth model to synthesize a more complex image texture. Pratt *et al.* [125, 148] developed a set of techniques for generating textures with identical means, variances, and autocorrelation functions but different

higher-order moments. Gagalowicz [149] gave a technique for generating binary texture fields with prescribed second-order statistics. Chellappa and Kashyap [150] described a technique for the generation of images having a given Gauss-Markov random field.

Yokoyama and Haralick [151] described a technique that uses a Markov chain method. Schachter [152] used a long, crested wave model. Monne *et al.* [153] used an interlaced vertical and horizontal Markov chain method to generate a texture image. Garber and Sawchuk [154] used a best fit model instead of the Nth-order transition probabilities to make good simulations of texture without exceeding computer memory limits on storing nth-order probability functions. Schmitt *et al.* [155] added vector quantization to the bidimensional Markov technique of Monne *et al.* [153] to improve the appearance of the texture image. Gagalowicz [156] described a texture synthesis technique that produces textures as they would appear on perspective projection images of three-dimensional surfaces. Ma and Gagalowicz [157] described a technique to synthesize artificial textures in parallel from a compressed data set and retain good visual similarity to natural textures.

REFERENCES

1. R. M. Haralick, Statistical and structural approaches to texture, *Proc. IEEE* **67**(5) 786-804 (May 1979).
2. N. Ahuja and A. Rosenfeld, Mosaic models for textures, *IEEE Transactions on Pattern Analysis and Machine Intelligence* **PAMI-3** (1) 1-11 (1981).
3. R. Ehrich and J. Foith, Topology and semantics of intensity arrays, *in* "Computer Vision" (Hanson and Riseman, eds.). Academic Press, New York, 1978.
4. H. Tamura, S. Mori and T. Yamawaki, Textural features corresponding to Visual Perception, *IEEE Transactions on Systems, Man, and Cybernetics* **SMC-8** (6), 460-473 (1978).
5. J. Bacus and E. Gose, Leukocyte pattern recognition, *IEEE Transactions on Systems, Man, and Cybernetics* **SMC-2** (4), 513-526 (1972).
6. R. M. Haralick and K. Shanmugam, Combined spectral and spatial processing of ERTS imagery data, *Proc. 2nd Symp. Significant Results Obtained from Earth Resources Technology Satellite-1, NASA SP-327, NASA Goddard Space Flight Center, Greenbelt, Maryland, Mar. 5–9, 1973*, pp. 1219-1228 (1973).
7. H. C. McDonald, Geologic evaluation of radar imagery from Darien province Panama, *CRES Technical Report* **133-6**, University of Kansas Center for Research, Inc., Lawrence, Kansas (1970).
8. R. M. Haralick and D. E. Anderson, Texture-tone study with application to digitized imagery, *CRES Technical Report* **182-2**, University of Kansas Center for Research, Inc., Lawrence, Kansas (November 1971).
9. A. J. Lewis, Geomorphic evaluation of radar imaging of southeastern Panama and northwestern Columbia, *CRES Technical Report* **133-18**, University of Kansas Center for Research, Inc., Lawrence, Kansas (February 1971).
10. A. M. Yaglom, "Theory of Stationary Random Functions." Prentice-Hall, Englewood Cliffs, New Jersey, 1962.
11. H. Kaizer, A quantification of textures on aerial photographs, *Tech Note* **121**, AD 69484, Boston University Research Laboratories, Boston University, Boston, Massachusetts, 1955.

12. G. Lendaris and G. Stanley, Diffraction pattern sampling for automatic pattern recognition, *SPIE Pattern Recognition Studies Seminar Proc., June 9–10, 1969*, pp. 127-154 (1969).
13. G. Lendaris and G. Stanley, Diffraction pattern samplings for automatic pattern recognition, *Proceedings of the IEEE* **58**, 198-216 (1970).
14. L. J. Cutrona, E. N. Leith, C. J. Palermo, and L. J. Porcello, Optical data processing and filtering systems, *IRE Transactions on Information Theory* **15** (6), 386-400 (1969).
15. J. W. Goodman, "Introduction to Fourier Optics." McGraw-Hill, New York, 1968.
16. K. Preston, "Coherent Optical Computers." McGraw-Hill, New York, 1972.
17. A. R. Shulman, "Optical Data Processing." Wiley, New York, 1970.
18. G. D. Swanlund, Design requirements for texture measurements, *Proc. Two Dimensional Digital Signal Processing Conf., Oct. 1971* (1971).
19. N. Gramenopoulas, Terrain type recognition using ERTS-1 MSS images, *Rec. Symp. Significant Results Obtained from the Earth Res. Technol. Satellite, NASA SP-327, Mar. 1973*, pp. 1229-1241.
20. R. J. Horning and J. A. Smith, Application of Fourier analysis to multispectral/spatial recognition, *Management and Utilization of Remote Sensing Data ASP Symposium, Sioux Falls, South Dakota, Oct. 1973* (1973).
21. R. Bajcsy, Computer identification of visual surfaces *Computer Graphics and Image Processing* **2**, 118-130 (1973).
22. R. Bajcsy and L. Lieberman, Computer description of real outdoor scenes, *Proc. 2nd Intl. Joint Conf. on Pattern Recognition, Copenhagen, Denmark, Aug. 1974*, pp. 174-179 (1974).
23. R. Bajcsy and L. Lieberman, Texture gradient as a depth cue, *Computer Graphics Image Processing* **5**, No. 1, 52-67 (1976).
24. R. M. Haralick, K. Shanmugam, and I. Dinstein, Textural features for image classification, *IEEE Transactions on Systems, Man, and Cybernetics* **SMC-3**, 610-621 (1973).
25. J. Weszka, C. Dyer, and A. Rosenfeld, A comparative study of texture measures for terrain classification, *IEEE Transactions on Systems, Man, and Cybernetics* **SMC-6** (4), 269-285 (1976).
26. R. W. Conners and C. A. Harlow, A theoretical comparison of texture algorithms, *IEEE Transactions on Pattern Analysis and Machine Intelligence* **PAMI-2** (3), 204-222 (1980).
27. C. Dyer and A. Rosenfeld, Fourier texture features: suppression of aperture effects, *IEEE Transaction on Systems, Man, and Cybernetics* **SMC-6**, 703-705 (1976).
28. F. D'Astous and M. E. Jernigan, Texture discriminant based on detailed measures of the power spectrum, *7th Intl. Conference on Pattern Recognition, Montreal, July 30–Aug. 2, 1984*, pp. 83-86 (1984).
29. A. P. Pentland, Fractal-based description of natural scenes, *IEEE Transactions on Pattern Analysis and Machine Intelligence* **PAMI-6** (6), 661-675 (1984).
30. B. B. Mandelbrot, "The Fractal Geometry of Nature" Freeman, San Francisco, California, 1982.
31. L. Kirvida, Texture measurements for the automatic classification of imagery, *IEEE Transactions on Electromagnetic Compatibility* **18**, 38-42 (1976).
32. G. E. Lowitz, Can a local histogram really map texture information? *6th Intl. Conference on Pattern Recognition, Munich, Germany, Oct. 19–22, 1982*, pp. 293-297 (1982).
33. G. E. Lowitz, Can a local histogram really map texture information?, *Pattern Recognition* **16**, No. 2, 141-147 (1983).
34. M. J. Carlotto, Texture classification based on hypothesis testing approach, *7th Intl. Conference on Pattern Recognition, July 30–Aug. 2, 1984*, pp. 93-96 (1984).
35. S. W. Zucker, Finding structure in co-occurrence matrices for texture analysis, *Computer Graphics and Image Processing* **12**, 286-308 (1980).
36. B. Julesz, Visual pattern discrimination, *IRE Transactions on Information Theory* **8** (2), 84-92 (1962).

37. A. L. Zobrist and W. B. Thompson, Building a distance function in Gestalt grouping, *IEEE Transaction on Computers* **C-4** (7), 718-728 (1975).
38. E. M. Darling and R. D. Joseph, Pattern recognition from satellite altitudes, *IEEE Transactions on Systems, Man, and Cybernetics* **SMC-4**, 38-47 (1968).
39. W. S. Deutsch and N. J. Belknap, Texture descriptors using neighborhood information, *Computer Graphics and Image Processing* **1**, 145-168 (1972).
40. P. H. Bartels and G. L. Wied, Extraction and evaluation of information from digitized cell images, "Mammalian Cells: Probes and Problems," U.S. Technical Information Center, Springfield, Virginia, 1975.
41. P. Bartels, G. Bahr, and G. Weid, Cell recognition from line scan transition probability profiles, *Acta Cytol* **13**, 210-217 (1969).
42. G. Weid, G. Bahr, and P. Bartels, Automatic analysis of cell images, *in* "Automated Cell Identification and Cell Sorting" (Weid and Bahr, eds.), pp. 195-360. Academic Press, New York, 1970.
43. A. Rosenfeld and E. Troy, Visual texture analysis, *Tech. Rep.* **70-116**, University of Maryland, College Park, Maryland, (June 1970). [Also in *Conference Record for Symposium on Feature Extraction and Selection in Pattern Recognition, Argonne, Illinois.* (IEEE Publication 70C-51C) *Oct. 1970*, pp. 115-124 (1970).]
44. R. M. Haralick, A texture-context feature extraction algorithm for remotely sensed imagery, *Proc. 1971 IEEE Decision and Control Conf., Gainesville, Florida, Dec. 15-17, 1971*, pp. 650-657 (1971).
45. M. M. Galloway, Texture analysis using gray level run lengths, *Comput. Graphic Image Process* **4**, 172-179 (1975).
46. P. C. Chen and T. Pavlidis, Segmentation by texture using a co-occurrence matrix and a split-and-merge algorithm, *Tech. Rep.* **237**, Princeton University, Princeton, New Jersey, (January, 1978).
47. J. T. Tou and Y. S. Chang, Picture understanding by machine via textural feature extraction, *Proc. 1977 IEEE Conf. on Pattern Recognition and Image Processing, Troy, New York, June 1977* (1977).
48. R. W. Conners and C. A. Harlow, Equal probability quantizing and texture analysis of radiographic images, *Computer Graphics and Image Processing*, **8**, 447-463 (1978).
49. R. M. Haralick and K. Shanmugam, Combined spectral and spatial processing of ERTS imagery data, *J. remote Sensing Environment* **3**, 3-13 (1974).
50. Y. P. Chien and K. S. Fu, Recognition of X-ray picture patterns, *IEEE Transactions on Systems, Man, and Cybernetics* **SMC-4** (2), 145-156 (1974).
51. N. J. Pressman, N. J. Markovian analysis of cervical cell images, *Journal of Histochem. Cytochem.* **24**, No. 1, 138-144 (1976).
52. N. J. Pressman, Optical texture analysis for automated cytology and histology: A Markovian approach, Unpublished dissertation, Lawrence Livermore Laboratory Report UCRL-52155, Livermore, California (1976).
53. A. L. Vickers and J. W. Modestino, A maximum likelihood approach to texture classification, *IEEE Transactions on Pattern Analysis and Machine Intelligence* **PAMI-4** (1), (1982).
54. A. Rosenfeld, C. Wang, and A. Y. Wu, Multispectral texture, *IEEE Transactions on Systems, Man, and Cybernetics* **SMC-12** (1), 79-84 (1982).
55. C. Sun and W. G. Wee, neighboring gray level dependence matrix for texture classification, *Computer Vision, Graphics, and Image Processing* **23**, 341-352 (1983).
56. H. Wechsler and M. Kidode, A random walk procedure for texture discrimination, *IEEE Transactions on Pattern Analysis and Machine Intelligence* **PAMI-1** (3), 272-280 (1979).
57. H. Wechsler and T. Citron, Feature extraction for texture classification, *Pattern Recognition* **12**, 301-311 (1980).
58. P. DeSouza, P. A note on a random walk model for texture analysis, *Pattern Recognition* **16**, No. 2, 219-283 (1983).

59. J. K. Percus, On the Wechsler-DeSouza discussion, *Pattern Recognition* **16**, No. 2, 269-270 (1983).
60. R. M. Haralick, A textural transform for images, *Proc. IEEE Conf. Computer Graphics, Pattern Recognition, and Data Structure, Beverly Hills, May 14–15, 1975* (1975).
61. R. W. Conners and C. A. Harlow, Some theoretical considerations concerning texture analysis of radiographic images, *Proc. 1976 IEEE Conf. on Decision and Control* (1976).
62. C. R. Dyer, T. Hong, and A. Rosenfeld, Texture classification using gray level cooccurrence based on edge maxima, *IEEE Transactions on Systems, Man, and Cybernetics* **SMC-10** (3), 158-163 (1980).
63. L. S. Davis, M. Clearman, and J. K. Aggarwal, An empirical evaluation of generalized cooccurrence matrices, *IEEE Transactions on Pattern Analysis and Machine Intelligence* **PAMI-3** (2), 214-221 (1981).
64. S. W. Zucker and K. Kant, Multiple-level representations for texture discrimination, *Pattern Recognition and Image Processing Conference, Dallas, Texas, Aug. 3–5, 1981*, pp. 609-614 (1981).
65. D. Terzopoulos and S. W. Zucker, Detection of osteogenesis imperfecta by automated texture analysis, *Computer Graphics and Image Processing* **20**, 229-243 (1982).
66. L. S. Davis, Polarograms: a new tool for image texture analysis, *Pattern Recognition* **13**, No. 3, 219-233 (1981).
67. D. Chetverikov, Textural anisotrophy features for texture analysis, *Pattern Recognition and Image Processing Conference, Dallas, Texas, Aug. 3–5, 1981*, pp. 583-588 (1981).
68. D. Chetverikov, Measuring the degree of texture regularity, *7th International Conference on Pattern Recognition*, Montreal, Canada, 80-82 (July 30-August 2 1984).
69. G. Matheron, "Elements Pour Une Theorie das Milieux Poreux." Masson, Paris, 1967.
70. J. Serra and G. Verchary, Mathematical morphology applied to fibre composite materials, *Film Sci. Tech.* **6**, 141-158 (1973).
71. W. Muller and W. Hunn, Texture analyzer system, *Industrial Research*, 49-54 (1974).
72. W. Muller, The Leitz texture analyzes systems, *Leitz Sci. Tech. Inform.*, Suppl. 1, No. 4, 101-136, Wetzlar, Germany (April 1974).
73. J. Serra, Theoretical bases of the Leitz texture analysis system, *Leitz Sci. Tech. Inform.* Suppl. 1, No. 4, 125-136 Wetzlar, Germany, (April 1974).
74. S. Sternberg, Parallel architectures for image processing, *Proceedings of COMPSAC, 1979* (1979).
75. G. S. Watson, *Geological Society of America Memoir* **142**, 367-391 (1975).
76. S. Sternberg, Biomedical image processing, *Computer* **16** No. 1, 22-34 (1983).
77. S. Peleg, J. Naor, R. Hartley, and D. Avnir, Multiple resolution texture analysis and classification, *IEEE Transactions on Pattern Analysis and Machine Intelligence* **PAMI-6** (4) (1984).
78. M. Werman and S. Peleg, Multiresolution texture signatures using min-max operators, *7th Intl. Conference on Pattern Recognition, Montreal, July 30–Aug. 2*, 1984, pp. 97-99 (1984).
79. F. Meyer, Iterative image transformations for an automatic screening of cervical smears, *J. Histochem. Cytochem.* **27**(1), 128-135 (1979).
80. Lipkin and Lipkin (1974).
81. G. Matheron, "Random Sets and Integral Geometry." Wiley, New York, 1975.
82. J. Serra, One, two, three, . . . , infinity, *in* "Quantitative Analysis of Microstructures in Materials Science, Biology, and Medicine" (J. L. Chernant, ed.), Riederer-Verlag, Stuttgart, Germany, pp. 9-24.
83. J. Serra, "Image Analysis and Mathematical Morphology." Academic Press, New York, 1982.
84. C. Lantuejoul, Grain dependence test in a polycrystalline ceramic, *in* "Quantitative Analysis of Microstructures in Materials Science, Biology, and Medicine" (J. L. Chernant, ed.), pp. 40-50. Riederer-Verlag, Stuttgart, 1978.

85. A. Rosenfeld and M. Thurston, Edge and curve detection for visual scene analysis, *IEEE Transactions on Computers* **C-20** (5), 562-569 (1971).
86. R. Sutton and E. Hall, Texture measures for automatic classification of pulmonary disease, *IEEE Transactions on Computers* **C-21**, No. 1, 667-676 (1972).
87. E. E. Triendl, Automatic terrain mapping by texture recognition, *Proceedings of the 8th Intl. Symposium on Remote Sensing of Environment*, Environmental Research Institute of Michigan, Ann Arbor, Michigan (October 1972).
88. S. Hsu, A texture-tone analysis for automated landuse mapping with panchromatic images, *Proc. Am. Soc. Photogrammetry*, 203-215 (March 1977).
89. G. H. Landerweerd and E. S. Gelsema, The use of nuclear texture parameters in the automatic analysis of leukocytes, *Pattern Recognition* **10**, 57-61 (1978).
90. A. Rosenfeld, A note on automatic detection of texture gradients, *IEEE Transactions on Computers* **C-23** (10), 998-991 (1975).
91. R. Harris and E. C. Barrett, Toward an objective nephanalysis *Journal of Applied Meteorology* **17**, 1258-1266 (1978).
92. D. Lu, J. T. Tou, and T. Gu, A simplified procedure for statistical feature extraction in texture processing, *IEEE Pattern Recognition and Image Processing Conference, Dallas Texas, August 3–5, 1981*, pp. 589-592 (1981).
93. H. C. Shen and A. K. Wong, Generalized texture representation and metric, *Computer Vision Graphics and Image Processing* **23**, 187-206 (1983).
94. R. S. Ledley, Texture problems in biomedical pattern recognition, *Proceedings of the 1972 IEEE Conf. on Decision and Control and the 11th Symposium on Adaptive Processes, New Orleans, Louisiana, Dec. 1972* (1972).
95. L. S. Rotolo, Automatic texture analysis for the diagnosis of pneumoconiosis, *26th ACEMB, Minneapolis, Minnesota, Sept. 30–Oct. 4, 1973*, p. 32 (1973).
96. O. Mitchell, C. Myers, and W. Boyne, A max-min measure for image texture analysis, *IEEE Transactions on Computers* **C-25**, 408-414 (1977).
97. S. G. Carlton and O. Mitchell, Image segmentation using texture and grey level, *Pattern Recognition and Image Processing Conference, Troy, New York, June, 1977*, pp. 387-391 (1977).
98. R. Ehrich and J. P. Foith, Representation of random waveforms by relational trees, *IEEE Transactions on Computers* **C-25**, 725-736 (1976).
99. M. O. M. Osman and T. S. Saukar, The measurement of surface texture by means of random function technique, ISA ASI 75262, American Institute of Aeronautics and Astronautics Technical Information Service A 76-14546, pp. 355-360 (1975).
100. R. Bachi, Geostatistical analysis of territories, *Proc. 39th Session—Bulletin of the Intl. Statistical Inst., Vienna, Austria, 1973*, (1973).
101. Y. S. Frolov, Measuring the shape of geographical phenomena: a history of the issue, *Sov. Geog.: Rev. Transl.* **16**, (10), 676-687 (1975).
102. W. Carel, W. Purdy, and R. Lulow, The VISILOG: A bionic approach to visual space perception and orientation, *Proceedings 1961 National Aerospace Electronics Conference (NAECON), Dayton, Ohio, May 8–10, 1961*, pp. 295-300 (1961).
103. P. W. Charton and E. E. Ferris, "The VISILOG: A synthetic eye," General Electric Company Technical report Al-TDR-64-185, DDC No. AD611539, January, 1965.
104. A. P. Witkin, Recovering surface shape and orientation from texture, *Artificial Intelligence* **17**, 17-45 (1981).
105. L. S. Davis, L. Janos, and S. Dunn, Efficient recovery of shape from texture, *IEEE Transactions on Pattern Analysis and machine Intelligence* **PAMI-5** (5), 485-492 (1983).
106. J. R. Kender, Shape from texture: An aggregation transform that maps a class of textures into surface orientation, *Int. Joint Conference on Artifician Intelligence, Tokyo, Japan, Aug. 20–23, 1979*, pp. 475-480 (1979).
107. C. K. Chow, A recognition method using neighbor dependence, *IRE Transactions on Electronic Computers* **11**, 683-690 (1962).

108. K. Abend, T. J. Harley, and L. N. Kanal, Classification of binary random patterns, *IEEE Transactions on Information Theory* **IT-11** (4) 538-544 (1965).
109. M. Hassner and J. Sklansky, The use of Markov random fields as models of texture, *Computer Graphics and Image Processing* **12**, 357-370 (1980).
110. J. W. Woods, Two-dimensional discrete Markovian fields, *IEEE Transactions on Information Theory* **IT-18**, 232-240 (1972).
111. J. E. Box and G. M. Jenkins, "Time Series Analysis" Holden-Day, San Francisco, California, 1970.
112. B. H. McCormick and S. N. Jayaramamurthy, Time series model for texture synthesis, *Int. J. Comput. Inform. Sci.* **3** (4) 329-343 (1974).
113. J. T. Tou and Y. S. Chang, An approach to texture pattern analysis and recognition, *Proc. 1976 IEEE Conf. on Decision and Control, 1976* (1976).
114. J. T. Tou, D. B. Kao, and Y. S. Chang, Pictorial texture analysis and synthesis, *3rd Intl. Joint Conf. on Pattern Recognition, Coronado, California, Nov. 1976*, pp. 590-590e (1976).
115. K. Deguchi and I. Morishita, Texture characterization and texture-based image partitioning using two-dimensional linear estimation techniques, *IEEE Transactions on Computers* **27**, No. 8, 739-745 (1978).
116. E. J. Delp, R. L. Kashyap, and O. R. Mitchell, Image data compression using autoregressive time series models *Pattern Recognition* **11**, 313-323 (1979).
117. J. T. Tou, Pictorial feature extraction and recognition via image modeling, *Computer Graphics and Image Processing* **12**, 376-406 (1980).
118. C. H. Chen, On two-dimensional ARMA models for image analysis, *5th Intl. Conference on Pattern Recognition, Miami, Florida, Dec. 1–4, 1980*, pp. 1129-1131 (1980).
119. O. D. Faugeras, Autoregressive modeling with conditional expectation or texture synthesis, *5th Intl. Conference on Pattern Recognition, Miami, Florida, Dec. 1–4, 1980*, pp. 792-794 (1980).
120. C. W. Therrien, Linear filtering models for texture classification and segmentation, *5th Intl. Conference on Pattern Recognition, Miami, Florida, Dec. 1–4, 1980*, pp. 1132-1135 (1980).
121. Y. C. Jau, R. T. Chin, and J. A. Weinman, Time series modeling for texture analysis and synthesis with application to cloud field morphology study, *7th Intl. Conference on Pattern Recognition, Montreal, Aug. 1984*, pp. 1219-1221 (1984).
122. R. L. Kashyap and R. Chellappa, Decision rules for choice of neighbors in random field models of images, *Computer Graphics and Image Processing* **15**, 301-318 (1981).
123. P. DeSouza, Texture recognition via autoregression, *Pattern Recognition* **15**, No. 6, 471-475 (1982).
124. W. K. Pratt, Image feature extraction, "Digital Image Processing," pp. 471-513, Wiley (Interscience), New York, 1978.
125. W. K. Pratt, O. D. Faugeras, and A. Gagalowicz, Visual discrimination of stochastic texture fields, *IEEE Transactions on Systems, Man, and Cybernetics* **SMC-8** (11), 796-804 (1978).
126. O. D. Faugeras and W. K. Pratt, Decorrelation methods of texture feature extraction, *IEEE Transactions on Pattern Analysis and Machine Intelligence* **PAMI-2** (4), 323-332 (1980).
127. K. Laws, Textured image segmentation, USCIPI Report 940, Image Processing Institute, University of Southern California (January 1980).
128. M. Unser, Local linear transforms for texture analysis, *7th Intl. Conference on Pattern Recognition, Montreal, July 30–Aug. 2, 1984*, pp. 1206-1208 (1984).
129. A. Ikonomopoulos and M. Unser, A directional filtering approach to texture discrimination, *7th Intl. Conference on Pattern Recognition, July 30–Aug. 2, 1984*, pp. 87-89 (1983).
130. M. E. Jernigan and F. D'Astous, Entropy-based texture analysis in the spatial frequency domain *IEEE Transactions on Pattern Analysis and machine Intelligence* **PAMI-6**, No. 2, 237-243 (March 1984).

131. R. Miles, Random polygons determined by random lines in the plane, *Proc. National Academy of Sciences U.S.A.* **52**, 901-907, 1157-1160 (1969).
132. R. Miles, On the homogeneous planar Poisson point-process, *Math. Biosciences* **6**, 85-127 (1970).
133. B. J. Schachter, A. Rosenfeld, and L. S. Davis, Random mosaic models for textures, *IEEE Transactions on Systems, Man, and Cybernetics* **SMC-8** (9), 694-702 (1978).
134. B. Schachter and N. Ahuja, Random pattern generation process, *Computer Graphics and Image Processing* **10**, 95-114 (1979).
135. N. Ahuja, T. Dubitzki, and A. Rosenfeld, Some experiments with mosaic models for images, *IEEE Transactions on Systems, Man, and Cybernetics* **SMC-10** (11), 744-749 (1980).
136. B. Schachter, Long crested wave models, *Computer Graphics and Image Processing* **12**, 187-201 (1980).
137. J. W. Modestino, R. W. Fries, and A. L. Vickers, Stochastic image models generated by random tessellations of the plane, *Computer Graphics and Image Processing* **12**, 74-98 (1980).
138. J. W. Modestino, R. W. Fries, and A. L. Vickers, Texture discrimination based upon an assumed stochastic texture model, *IEEE Transactions on Pattern Analysis and Machine Intelligence* **PAMI-3** (5) 557-580 (1981).
139. C. W. Therrien, An estimation-theoretic approach to terrain image segmentation, *Computer Vision, Graphics and Image Processing* 22, 313-326 (1983).
140. E. Gilbert, Random subdivisions of space into crystals, *Annals Math. Stat.* **33**, 958-972 (1962).
141. P. Switzer, Reconstructing patterns for sample data, *Annals Math. Stat.* **38**, 138-154 (1967).
142. R. Bajcsy, Computer description of textured surfaces, *3rd Intl. Joint Conf. on Artificial Intelligence, Stanford, California, Aug. 20–23, 1973*, pp. 572-578 (1973).
143. T. Hong, A. Wu, and A. Rosenfeld, Feature value smoothing as an aid in texture analysis, *IEEE Transactions on Systems, Man, and Cybernetics* **SMC-10**, No. 8, 519-524 (August 1980).
144. P. C. Chen and T. Pavlidis, Segmentation by texture using correlation *IEEE Transactions on Pattern Analysis and Machine Intelligence* **PAMI-5** (1), 64-69 (1983).
145. R. W. Conners, Trivedi, and C. A. Harlow, (1984).
146. R. L. Kashyap and A. Khotanzad, A stochastic model based technique for texture segmentation *7th int. Conference on Pattern Recognition, Montreal, July 30–Aug. 2, 1984*, pp. 1202-1205 (1984).
147. Yokoyama and Haralick, Texture synthesis using a growth model, *Computer Graphics and Image Processing* **8**, 369-381 (1978).
148. W. K. Pratt, O. D. Faugeras, and A. Gagalowicz, Applications of stochastic texture field models to image processing, *Proceedings of the IEEE* **69** (5), 542-551 (1981).
149. A. Gagalowicz, A new method for texture fields synthesis: some applications to the study of human vision, *IEEE Transactions on Pattern Analysis and Machine Intelligence* **PAMI-3** (5), 520-533 (1981).
150. R. Chellappa and R. L. Kashyap, Synthetic generation and estimation in random field models of images, *Proceedings of the 1981 Pattern Recognition and Image Processing Conference, Dallas, Texas, Aug. 3–5*, pp. 577-582 (1981).
151. Yokoyama and Haralick, Texture pattern image generation by regular Markov chains, *Pattern Recognition* **11**, 225-254 (1979).
152. B. Schachter, Model based texture measures, *IEEE Transactions on Pattern Analysis and Machine Intelligence* **PAMI-2** (2), 169-171 (1980).
153. J. Monne, F. Schmitt, and C. Massaloux, Bidimensional texture synthesis by Markov chains, *Computer Graphics and Image Processing* **17**, 1-23 (1981).

154. D. Garber and A. A. Sawchuk, Texture simulation using a best fit model, *Pattern Recognition and Image Processing Conference, Dallas, Texas, Aug. 3–5, 1981*, pp. 603–608.
155. F. Schmitt, M. Goldberg, N. Ngwa-Ndifor, and P. Baucher, Texture representation and synthesis, *7th Intl. Conference on Pattern Recognition, Montreal, July 30–Aug. 2, 1984*, pp. 1222–1225 (1984).
156. A. Gagalowicz, Synthesis of natural textures on 3-D surfaces, *7th Intl. Conference on Pattern Recognition, Montreal, July 30–Aug. 2, 1984*, pp. 1209–1212 (1984).
157. Ma. S. and A. Gagalowicz, A parallel method for natural texture synthesis, *7th Intl. Conference on Pattern Recognition, Montreal, July 30–Aug. 2, 1984*, pp. 90–92 (1984).